Cellular/Molecular

β-Secretase BACE1 Regulates Hippocampal and Reconstituted M-Currents in a β-Subunit-Like Fashion

Sabine Hessler,[1] Fang Zheng,[1] Stephanie Hartmann,[1] Andrea Rittger,[2] Sandra Lehnert,[1] Meike Völkel,[3] Matthias Nissen,[1] Elke Edelmann,[3,4] Paul Saftig,[2] Michael Schwake,[2,5] Tobias Huth,*[1] and Christian Alzheimer*[1]

[1]Institute of Physiology and Pathophysiology, Friedrich-Alexander-Universität Erlangen-Nürnberg, 91054 Erlangen, Germany, [2]Institute of Biochemistry, Christian-Albrechts-Universität, 24098 Kiel, Germany, [3]Institute of Physiology, Christian-Albrechts-Universität, 24098 Kiel, Germany, [4]Institute of Physiology, Otto-von-Guericke-Universität Magdeburg, 39120 Magdeburg, Germany, and [5]Biochemie III, Fakultät für Chemie, Universität Bielefeld, 33615 Bielefeld, Germany

The β-secretase BACE1 is widely known for its pivotal role in the amyloidogenic pathway leading to Alzheimer's disease, but how its action on transmembrane proteins other than the amyloid precursor protein affects the nervous system is only beginning to be understood. We report here that BACE1 regulates neuronal excitability through an unorthodox, nonenzymatic interaction with members of the KCNQ (Kv7) family that give rise to the M-current, a noninactivating potassium current with slow kinetics. In hippocampal neurons from BACE1 $^{-/-}$ mice, loss of M-current enhanced neuronal excitability. We relate the diminished M-current to the previously reported epileptic phenotype of BACE1-deficient mice. In HEK293T cells, BACE1 amplified reconstituted M-currents, altered their voltage dependence, accelerated activation, and slowed deactivation. Biochemical evidence strongly suggested that BACE1 physically associates with channel proteins in a β-subunit-like fashion. Our results establish BACE1 as a physiologically essential constituent of regular M-current function and elucidate a striking new feature of how BACE1 impacts on neuronal activity in the intact and diseased brain.

Key words: **Alzheimer's disease; BACE1; epilepsy; hippocampus; KCNQ; M-current**

Introduction

The M-current (I_M) was first described in bullfrog sympathetic neurons as a noninactivating voltage-dependent K^+ current with slow activation and deactivation kinetics that could be suppressed by muscarine, hence its name (Brown and Adams, 1980). Because of its low voltage range for activation, I_M generates a standing outward current below firing threshold that exerts a strong potential-clamping effect. By now, I_M has been identified in numerous neurons of the peripheral and CNS (Jentsch, 2000; Brown and Passmore, 2009; Passmore et al., 2012). Depending on its subcellular location, a number of different electrophysiological functions have been attributed to I_M (Yue and Yaari, 2006; Shah et al., 2011). For example, perisomatic I_M of hippocampal, entorhinal, and neocortical neurons has been shown to delay the onset of firing during ramp depolarization, to reduce the firing rate during sustained depolarization, to modulate subthreshold integration of synaptic inputs, and to contribute to subthreshold membrane oscillations and electrical resonance at theta frequency (Hu et al., 2002; Peters et al., 2005; Otto et al., 2006; Hu et al., 2007; Guan et al., 2011). Because of its relatively slow kinetics, I_M does not participate appreciably in action potential (AP) repolarization, but it mediates, in many neurons, an afterhyperpolarization of medium duration (Gu et al., 2005; Tzingounis and Nicoll, 2008). I_M is also present in axons and presynaptic terminals, where it modulates firing patterns and transmitter release, respectively (Martire et al., 2004; Vervaeke et al., 2006; Sun and Kapur, 2012; Battefeld et al., 2014).

Four of the five members of the KCNQ/Kv7 family (KCNQ2–5) can assemble in different combinations to generate I_M (Brown and Passmore, 2009). Outside the auditory system, in which KCNQ4 is prominently expressed (Jentsch, 2000; Leitner et al., 2012), M-channels appear to be predominantly formed by heteromeric assemblies of KCNQ2/KCNQ3 and KCNQ3/KCNQ5, although all KCNQ members can give rise to homomeric channels *in vitro* (Wang et al., 1998; Lerche et al., 2000; Schroeder et al., 2000; Shah et al., 2002; Schwake et al., 2006; Brown and Passmore, 2009). We report here the striking finding that the β-secretase BACE1 (β-site APP-cleaving enzyme 1) is an important constituent of proper M-channel function. Importantly, the augmenting effect of BACE1 on I_M occurs independently of its proteolytic activity.

Over the last years, BACE1 has garnered ever-increasing attention, reflecting its pivotal role in the amyloidogenic pathway

Received July 29, 2014; revised Jan. 7, 2015; accepted Jan. 9, 2015.

Author contributions: S. Hessler, F.Z., S. Hartmann, A.R., S.L., P.S., M.S., T.H., and C.A. designed research; S. Hessler, F.Z., S. Hartmann, A.R., S.L., M.V., M.N., E.E., and T.H. performed research; S. Hessler, F.Z., S. Hartmann, A.R., S.L., and T.H. analyzed data; T.H. and C.A. wrote the paper.

This work was supported by Deutsche Forschungsgemeinschaft INST 90/675-1 FUGG to C.A., the Johannes und Frieda Marohn-Stiftung to T.H. and C.A., the Staedtler-Stiftung to C.A., the ELAN program of the Universitätsklinikum Erlangen to T.H., and the Studienstiftung des deutschen Volkes to S.L. and S. Hartmann. We thank Yasushi Okamura for providing the DR-VSP and DR-VSP C302S constructs; and Iwona Izydorczyk, Anette Wirth-Hücking, Didier Gremelle, Annette Kuhn, and Susi Haux-Oertel for technical assistance.

The authors declare no competing financial interests.

*T.H. and C.A. contributed equally to this study as senior authors.

Correspondence should be addressed to either Dr. Tobias Huth or Dr. Christian Alzheimer, Institute of Physiology and Pathophysiology, Friedrich-Alexander-Universität Erlangen-Nürnberg, Universitätsstr. 17, 91054 Erlangen, Germany. E-mail: tobias.huth@fau.de or christian.alzheimer@fau.de.

DOI:10.1523/JNEUROSCI.3127-14.2015

 0270-6474/15/353298-14$15.00/0

that has been closely linked to the pathogenesis of Alzheimer's disease (AD) (Vassar et al., 2014). Inhibition of BACE1 has therefore emerged as a prime therapeutic strategy to reduce the load of the potentially toxic amyloid β-peptide (Aβ) (Yan and Vassar, 2014). It is equally important, however, to understand the physiological functions of the secretase in the normal brain. We posit here that BACE1 associates with molecular correlates of I_M in an accessory subunit-like fashion, resembling the augmenting effect that the accessory subunit KCNE1 exerts on cardiac KCNQ1 channels (Sanguinetti et al., 1996).

Materials and Methods

Animals. BACE1 $^{-/-}$ mice (BACE1 ^{tm1Psa}) were generated by insertion of a neo expression cassette from pMC1neopA into exon 1 of *Bace1*. The insertion of the neo cassette introduces a premature translational stop codon into the open reading frame of the *Bace1* gene (Dominguez et al., 2005). Mice had *ad libitum* access to food and water and were housed and fed according to federal guidelines. PCR amplification was used to genotype mice either detecting wild-type allele or the neo cassette at P10-P12.

Plasmids. The following cDNA constructs were used in this work: hKCNQ2, hKCNQ2 W236L, hKCNQ3, hKCNQ3 A315T, hKCNQ2-V5, hKCNQ2-HA, hKCNQ3-HA (NM_004518.4 with rs1801475, NM_004519.2); hKCNQ4 (NM_004700.2 kindly provided by Thomas J. Jentsch, Leibniz-Institut für Molekulare Pharmakologie and Max-Delbrück-Centrum für Molekulare Medizin, Berlin, Germany); hKCNQ5 (NM_019842.2 kindly provided by Klaus Steinmeyer, R&D Aging/Quality of Life, Sanofi-Aventis, Frankfurt am Main, Germany); hBACE1, hBACE1-Flag, hBACE1 D289N (NM_012104.4, kindly provided by Michael Willem, Adolf-Butenandt-Institute, Ludwig-Maximilians-Universität München, München, Germany); hBACE2 (NM_012105.3) in pCMV6-XL5; DR-VSP and DR-VSP-C302S in pIRES2-EGFP (kindly provided by Yasushi Okamura, Laboratory of Integrative Physiology, Osaka University, Japan); hENaC1α-V5 and hENaC1α-HA (NM_001038.5, kindly provided by Christoph Korbmacher, Institute of Cellular and Molecular Physiology, Friedrich-Alexander-Universität Erlangen-Nürnberg, Erlangen, Germany, with permission from Harry Cuppens, Centre For Human Genetics, University of Leuven, Leuven, Belgium); pEGFP-C1 (Clontech), hMaxiK-GFP. All constructs were based on pcDNA3.1, if not stated otherwise.

Antibodies. The following antibodies were used in this work: mouse-anti-Flag (M2, Sigma-Aldrich); rat-anti-HA-POD (3F10, Roche); mouse-anti-BACE1 (10B8, kindly provided by Robert Vassar, Department of Cell and Molecular Biology, Northwestern University, Chicago); goat-anti-BACE1 (ab11028, Abcam); rabbit-anti-V5 (ab9116, Abcam); goat-anti-HA (ab9134, Abcam); rabbit-anti-KCNQ2; sheep-anti-KCNQ3; rabbit-anti-Na^+/K^+-ATPase α1 (#3010, Cell Signaling Technology); rabbit-anti-pan-cadherin (#4068, Cell Signaling Technology); mouse-anti-β-actin-HRP (A3854, Sigma-Aldrich); goat-anti-rabbit-IgG-HRP (ab6721, Abcam); and rabbit-anti-goat-IgG-HRP (ab6741, Abcam).

Cell culture and transient transfection. For maintenance, HEK293T cells (ATCC accession number CRL-11268, ATCC; www.atcc.org) were cultured in DMEM (1 g/L glucose; Invitrogen), supplemented with 10% FCS (Biochrom AG) and 1% penicillin/streptomycin (PAA), and were split every 3–4 d. For electrophysiological recordings, HEK293T cells were plated on 35 mm dishes (BD Bioscience) 1 d before transfection. These cells were transfected with Nanofectin (PAA) according to the manufacturer's protocol using 1 μg of cDNA and 0.5 μg of EGFP. For the proximity ligation assay (PLA), cells were plated on 12-well tissue culture plates (VWR) and transfected after 1 d with JetPEI (Polyplus-Transfection SA) using 250 ng DNA (125 ng each for channel constructs or BACE1). The next day, cells were split and plated on round 18 mm 1.5H coverslips. For coimmunoprecipitation and surface biotinylation, cells were plated on 100 mm tissue culture dishes (BD Bioscience) the day before transfection. The cells were transfected with JetPEI using 375 ng EGFP, 750 ng for each channel construct, and 1250 ng BACE1.

Coimmunoprecipitation. Cells were lysed in chilled EBC-buffer (50 mM Tris-HCl, 120 mM NaCl, 0,5% NP-40, pH 7.4) supplemented with protease inhibitors (Roche), followed by 2× mild sonication and 30 min incubation on ice. The lysate was centrifuged for 10 min at 4°C and 6000 × *g*. The protein concentration of the supernatant was measured with Bradford reagent and diluted to 1 μg/μl with PBS. A total of 500 μl protein solution was incubated with 1–2 μg of mouse-anti-BACE1-antibody at 4°C in an orbital shaker overnight. The 40 μl of magnetic beads solution (Thermo Fisher Scientific) were washed with PBS and blocked with 1% BSA for 1 h at room temperature. The beads were incubated for 15 min with the probe in an orbital shaker at room temperature followed by 5 times washing with PBS. Proteins were eluted with 65 μl Lämmli buffer at 55°C for 20 min.

Cell surface biotinylation. Biotinylation was conducted on ice/4°C. At 48 h after transfection, cells were washed three times with ice-cold Hank's balanced salt solution (HBSS with calcium and magnesium, Invitrogen) and incubated in the dark for 30 min with HBSS containing 0.3 mg/ml EZ-Link Sulfo-NHS-LC-LC-Biotin (Pierce). The reaction was stopped by incubation with 100 μM L-lysine in HBSS for 5 min followed by washing with HBSS. Next, cells were extracted in a lysis buffer containing 10 mM Tris-HCl, pH 7.6, 2 mM EDTA, pH 8.0, 150 mM NaCl (C. Roth), 0.2% SDS, 0.5% sodium deoxycholate, 1% Triton X-100, 1 mM 1–10-phenanthroline, and protease inhibitor mixture (Roche); pH 7.6. For homogenization, cell lysates were centrifuged at 1000 rpm, 6 min using shredder columns (QIAGEN) and sonicated for 5 min. To remove insoluble fractions, the lysates were centrifuged at 13,000 rpm for 15 min. Protein concentration was measured using the BCA Protein Assay Kit (Pierce). For total cell lysate samples, 20 μg of protein was prepared with 4× loading dye (Lonza) and 5% dithiothreitol. For biotinylation samples, 400 μg (1 μg/μl in extraction buffer) of protein was captured overnight by 30 μl of NeutrAvidin beads (Pierce) that had been washed in extraction buffer. The following day, the beads were washed three times with extraction buffer and captured proteins were eluted at 95°C for 5 min in a total volume of 50 μl consisting of extraction buffer, 4× loading dye and 5% dithiothreitol. Then, 15 μl was loaded for SDS-PAGE.

SDS-PAGE and Western blot analysis. Samples were heated at 95°C for 5 min. Proteins were separated in 10% SDS gels and transferred onto PVDF membranes (Bio-Rad). After blocking, primary antibodies were incubated overnight at 4°C in 1% BSA and 0.1% NaN_3. The membranes were incubated with secondary antibody coupled to HRP in 5% milk for 1 h at room temperature. The signal was visualized by enhanced chemiluminescence using SuperSignal West Pico Chemiluminescent Substrate (Pierce) or Clarity Western ECL Substrate (Bio-Rad) and imaged using the ChemoStar Imager (INTAS). Membranes were reprobed after stripping: 6 M guanidine-HCl (C. Roth), 20 mM Tris, 0.2% Triton X-100, pH 7.5, and 0.8% β-mercaptoethanol (C. Roth). Western blot signals were quantified using the ImageJ software (Wayne Rasband, Research Services Branch, National Institute of Mental Health, Bethesda, MD).

PLA. The Proximity Ligation Assay (PLA, Olink Bioscience) is a sensitive and specific assay for detection of protein-protein interactions within a maximum distance of 40 nm (Söderberg et al., 2006). After labeling two probable interaction partners by respective primary antibodies, the PLA produces fluorescent signals at the sites of interaction. Two days after transfection, cells were fixed with 4% PFA (C. Roth), 1.44% $Na_2HPO_4 \times 2H_2O$, 0.26% $NaH_2PO_4 \times 1H_2O$ for 10 min at room temperature. Antigens were retrieved in antigen retrieval buffer containing 100 mM Tris, 5% urea at pH 9.5 with HCl at 50°C for 10 min. Blocking was performed by incubation with PBT buffer containing 0.8% NaCl, 0.177% $Na_2HPO_4 \times 2H_2O$, 0.02% KH_2PO_4, 0.02% KCl, 1% BSA, 0.5% Triton X-100, pH 7.4, for 30 min with gentle shaking. After removal of blocking solution, reaction area was limited by staining masks that were made of Teflon in the in-house workshop. Masks were coated with high vacuum silicone grease (VWR) and gently sealed onto the coverslips with concentric pressure. The PLA was performed based on the manufacturer's protocol except for reagent volumes (20 μl) and a modified washing protocol (3–4 × with 50 μl). Primary antibodies were diluted in PBT, and samples were incubated for 2 h at room temperature with gentle shaking. Finally, samples were mounted with Duolink In Situ Mounting Medium with DAPI (Sigma-Aldrich). PLA samples were imaged with a confocal LSM 780 with an inverse stage Axio Observer.Z1 and Plan-Apochromat 63×/1.40 NA Oil DIC M27 objective (Carl Zeiss). Optical

slices of 1 airy unit were recorded using a 405 nm laser diode (DAPI) and a 561 nm laser line (PLA signals). For analysis, CellProfiler2.1.0, revision 0c7fb94 (Carpenter et al., 2006), was used. A template from Carolina Wählby (Centre for Image Analysis, Uppsala University, Sweden and Broad Institute of Harvard and Massachusetts Institute of Technology) served as basis for the processing pipeline, which is available upon request.

Hippocampal slice recordings. Mice of either sex were anesthetized with halothane and decapitated. All procedures were performed according to the guidelines and with the approval of the local government. Transverse hippocampal slices of 350 μm thickness were prepared from the brain of 15–30-d-old mice in ice-cold solution of the following composition (in mM): 75 sucrose, 87 NaCl, 2.5 KCl, 0.5 $CaCl_2$, 7.0 $MgCl_2$, 1.25 NaH_2PO_4, 25 $NaHCO_3$, and 10 D-glucose (bubbled with 95% O_2/5% CO_2, pH 7.4). Slices were transferred into warmed modified aCSF (35°C) containing (in mM) the following: 125 NaCl, 3 KCl, 0.5 $CaCl_2$, 7 $MgCl_2$, 1.25 NaH_2PO_4, 25 $NaHCO_3$, and 10 D-glucose (bubbled with 95% O_2/5% CO_2, pH 7.4) for 10 min and kept in aCSF solution with 0.5 $CaCl_2$ and 3.5 $MgCl_2$ at room temperature. Individual slices were transferred to a submerged recording chamber (perfused with aCSF containing (in mM) the following: 2.5 $CaCl_2$ and 1.0 $MgCl_2$ at 32°C) that was mounted on the stage of an upright microscope (Carl Zeiss). Whole-cell recordings from hippocampal CA1 pyramidal cells were performed using patch pipettes filled with (in mM) the following: 135 K-gluconate, 4 NaCl, 10 KCl, 5 HEPES, 5 EGTA, 2 Na_2-ATP, and 0.3 Na_3-GTP (pH 7.25). Voltage readings were corrected for liquid junction potentials. Unless stated otherwise, membrane potential in current-clamp mode was held at −70 mV by hyperpolarizing current injection. APs were evoked by depolarizing current steps of variable amplitude and duration. Membrane input resistance (R_N) was determined from the current response to a 5 mV hyperpolarizing voltage step. Data were collected with a Multiclamp 700B amplifier in conjunction with Digidata 1440A interface and pClamp10 software (Molecular Devices). Signals were digitized at 20 kHz and filtered at 5 kHz.

Recordings from acutely isolated CA1 pyramidal cells. Hippocampal CA1 neurons were freshly isolated from 14–17-d-old mice of either sex using a combined enzymatic/mechanic dissociation procedure. Transverse hippocampal slices (thickness: 350 μm for wt mice, 450 μm for BACE1$^{-/-}$) were kept in ice-cold sucrose solution (see above). After incubation at 32°C in warmed sucrose solution for 20–30 min, the slices were transferred into modified aCSF containing (in mM) the following: 125 NaCl, 3 KCl, 0.5 $CaCl_2$, 3.5 $MgCl_2$, 1.25 NaH_2PO_4, 25 $NaHCO_3$, and 10 D-glucose for 30 min. The CA1 region was prepared from slices and incubated in 1 mg/ml papain at 30°C for 25–30 min, constantly gassed with O_2. CA1 slices were washed 3–4 times with bath solution (see below) and kept for not >4 h in gassed bath solution. Cells were triturated from small pieces of CA1 slice tissue using pipettes with subsequently narrowing diameters in a solution containing (in mM) the following: 125 NaCl, 3 KCl, 1 $CaCl_2$, 10 $MgCl_2$, 10 HEPES, 10 Na-HEPES, 10 EGTA, 10 D-glucose, and 2 kynurenic acid. Dissociated cells were allowed to settle for 20–25 min before whole-cell recordings were started. Isolated CA1 pyramidal neurons were identified on the stage of the patch-clamp microscope using Hoffman modulation contrast optics. Patch pipettes were filled with (in mM) the following: 135 K-gluconate, 4 NaCl, 10 KCl, 5 HEPES, 5 EGTA, 2 Na_2-ATP, 0.3 Na_3-GTP (pH 7.25 with KOH). Bath solution contained (in mM) the following: 145 NaCl, 4 KCl, 2 $MgCl_2$, 2 $CaCl_2$, 10 HEPES, and 10 D-glucose, adjusted to pH 7.4 with NaOH. Voltage readings were corrected for liquid junction potentials. Cells were recorded at room temperature (22 ± 1°C) in whole-cell voltage-clamp mode as described for transfected HEK293T cells (see below).

Electrophysiology of transfected HEK293T cells. HEK293T cells were recorded 2 d after transfection and identified by their green fluorescence using an inverted fluorescence microscope (Axiovert 40, Carl Zeiss) combined with a fiber optic-coupled light source (UVICO, Rapp Opto-Electronic). Whole-cell recordings were performed at room temperature (22 ± 1°C), if not otherwise stated, using an Axopatch 700B amplifier in conjunction with a Digidata 1322A interface and pClamp 10 software (all from Molecular Devices). Borosilicate glass electrodes with filament (Biomedical Instruments) were pulled on a DMZ-Universal Puller (Zeitz) and had a tip resistance in bath solution of 1.8–2.5 MΩ. Series resistance compensation was ≧75%. Recordings were sampled at 20 kHz and filtered at 5 kHz. Experiments were started 3 min after whole-cell access was established. A gravity-driven Y-tube application system was used for exchanging external solutions. Patch electrodes were filled with (in mM) the following: 5 NaCl, 120 KCl, 2 $MgCl_2$, 1 $CaCl_2$, 10 HEPES, and 5 EGTA adjusted to pH 7.2 with KOH. Voltage readings were not corrected for liquid junction potentials. Bath solution contained (in mM) the following: 145 NaCl, 4 KCl, 2 $MgCl_2$, 2 $CaCl_2$, 10 HEPES, and 10 D-glucose, adjusted to pH 7.4 with NaOH. High K^+ bath solution contained (in mM) the following: 5 NaCl, 150 KCl, 2 $MgCl_2$, 2 $CaCl_2$, 10 HEPES, and 10 D-glucose, adjusted to pH 7.4 with KOH.

Data analysis of recordings from transfected HEK293T cells. From the activation protocols, the whole-cell potassium conductance G was calculated after leak correction for every command potential V according to the following equation:

$$G = \frac{I}{V - E_{rev}}.$$

The equilibrium potential E_{rev} for potassium was −85.7 mV under our experimental conditions. G was normalized and fitted with a Boltzmann equation of the form as follows:

$$G_{norm} = 1 \Big/ \left[1 + \exp\left(- \frac{V - V_{mid}}{k} \right) \right]$$

Activation time constants were estimated by using a single-exponential function with sloping baseline of the form as follows:

$$I(t) = A * e^{\frac{-t}{\tau}} + mt + I_0,$$

where A is current amplitude and m a sloping baseline factor accounting for the slight inactivation in recordings with BACE1. Deactivation time constants were estimated using a single-exponential function. Raw data analysis and fitting were performed with pClamp 10 (Molecular Devices).

Reagents. If not stated otherwise, reagents were purchased from Sigma-Aldrich.

Statistics. Statistical analysis was performed with Origin9.0Pro software (OriginLab). Numbers are given as mean ± SEM. Tests to determine statistical significance are stated in text or figure legends.

Results

Enhanced excitability of BACE1-deficient CA1 pyramidal cells results from diminished I_M

To examine the effects of BACE1 on intrinsic firing properties, we performed whole-cell current-clamp recordings from CA1 pyramidal neurons in hippocampal slices from wild-type (wt) and BACE1$^{-/-}$ mice. Resting membrane potential (RMP) and membrane input resistance (R_N) did not significantly differ between wt neurons ($n = 33$) and BACE1$^{-/-}$ neurons ($n = 25$) (RMP wt −66 ± 1 mV, BACE1$^{-/-}$ −67 ± 1 mV, $p = 0.77$; R_N wt 299 ± 18 MΩ, BACE1$^{-/-}$ 328 ± 25 MΩ, $p = 0.26$, unpaired t test). Injection of suprathreshold depolarizing current steps for 1 s evoked a pattern of repetitive AP discharges that displayed frequency adaptation during sustained depolarization (Fig. 1*A*). BACE1$^{-/-}$ neurons consistently showed a stronger firing response than wt neurons, as illustrated in Figure 1*B*. We quantified this effect by counting the overall number of spikes per depolarization for three different amplitudes of current injection (Fig. 1*C*) and by measuring the time to first AP after the start of the depolarizing current pulse (Fig. 1*D*). Except for the strongest current pulse, BACE1$^{-/-}$ neurons fired more spikes and displayed a shorter latency to first spike than wt neurons.

We next quantified and compared the voltage trajectories of APs in both preparations using the first AP elicited during a 50 pA

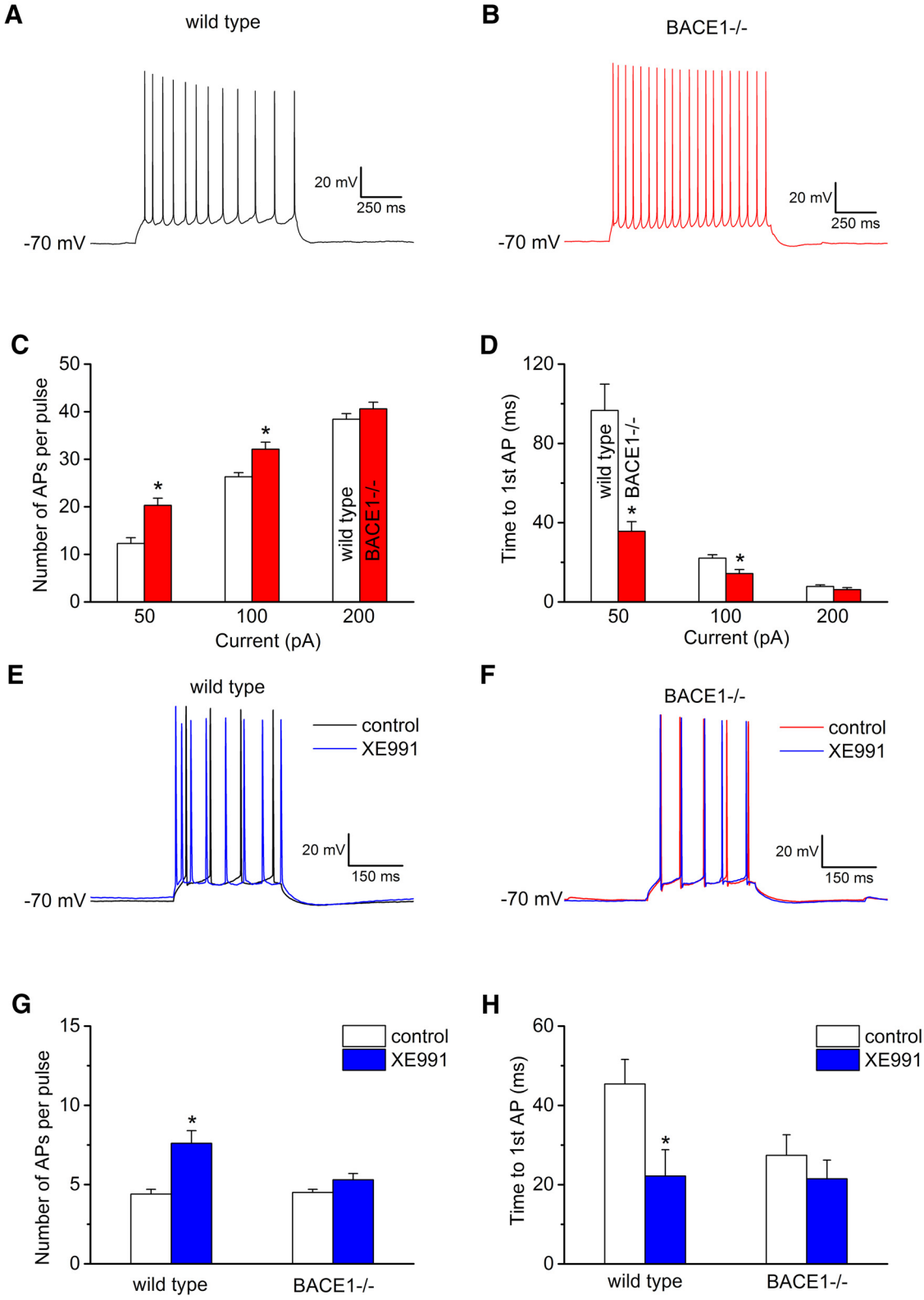

Figure 1. Reduced M-current (I_M) accounts for enhanced excitability of hippocampal CA1 pyramidal neurons from BACE1 $^{-/-}$ mice. Whole-cell current-clamp recordings from CA1 pyramidal neurons in hippocampal slices demonstrated that the characteristic frequency adaptation that gradually slows repetitive firing during sustained depolarization under normal conditions (***A***) is strongly attenuated in the absence of BACE1 (***B***). For comparison, membrane potentials were set to −70 mV before depolarizing current of equal size (50 pA) was injected. Histograms quantify number of APs (***C***) and time to first AP (***D***) during depolarizing steps of increasing amplitude for wt neurons (white columns, $n = 33$) and BACE1-deficient neurons (red columns, $n = 25$). *$p < 0.05$ (unpaired t test). Whereas XE991 (10 μM) reliably impaired frequency adaptation in wt neurons (***E***), the blocker failed to excite BACE1-deficient neurons (***F***). Again, membrane potential was set to −70 mV before firing. The amplitude of injected current was adjusted to elicit 4–5 APs during a 300 ms pulse before XE991 application. Histograms quantify number of APs (***G***) and time to first AP (***H***) during step depolarization for wt neurons ($n = 8$) and BACE1-deficient neurons ($n = 5$). *$p < 0.05$ (paired t test).

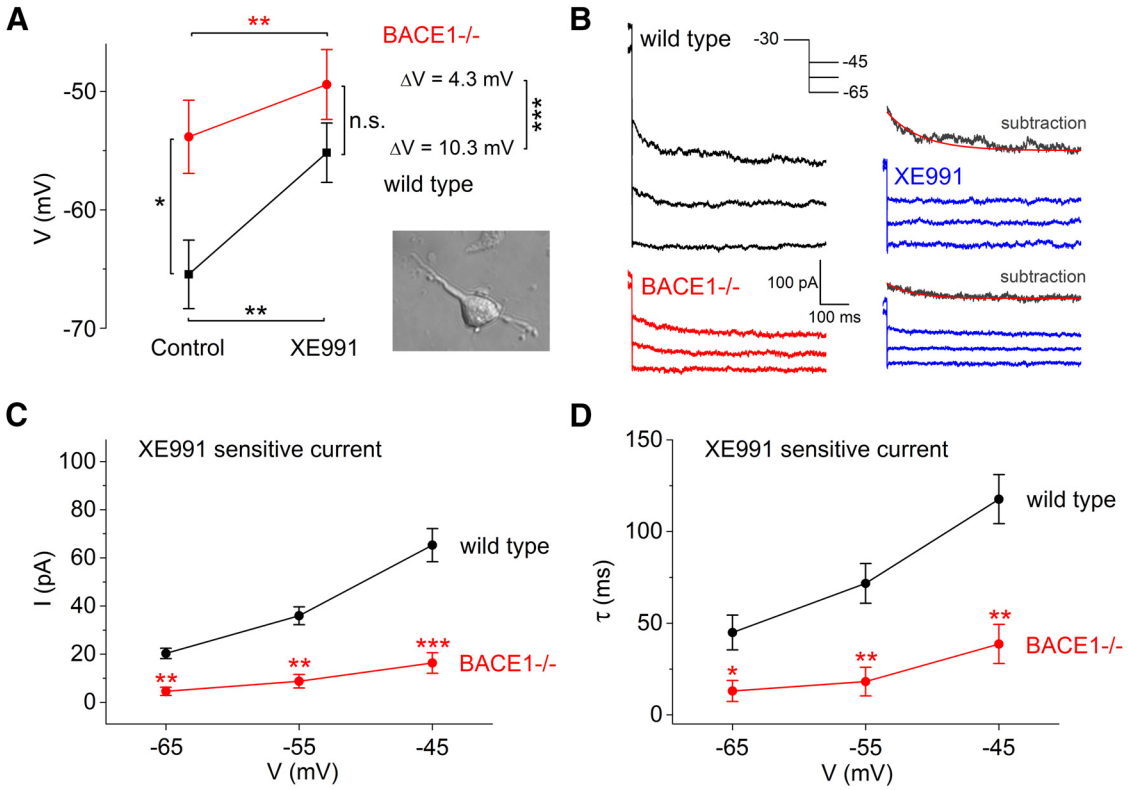

Figure 2. Acutely isolated CA1 pyramidal cells of BACE1 $^{-/-}$ mice show reduced I_M. ***A***, The significant difference in zero-current potential between wt and BACE1-deficient neurons disappeared in the presence of 10 μM XE991. ΔV, Drug-induced voltage shifts. Inset, Acutely isolated neuron. ***B***, Small hyperpolarizing voltage steps from −30 mV (inset) were used to interrogate I_M of wt (black traces) and BACE1 $^{-/-}$ neurons (red traces) in the absence and presence of 10 μM XE991 (blue traces). Traces above the latter represent XE991-subtracted current at −45 mV with fitted curve superimposed. At all voltages examined, the XE991-sensitive current of BACE1 $^{-/-}$ neurons (red data points) had smaller amplitudes (***C***) and faster deactivation kinetics (***D***) than that of wt neurons (black data points). Wt, $n = 11$; BACE1 $^{-/-}$, $n = 12$. *$p < 0.05$, **$p < 0.01$, ***$p < 0.01$, paired or unpaired t test, as applicable.

depolarizing current injection. The maximum slope during the rising phase of APs was slightly, but significantly, enhanced in BACE1 $^{-/-}$ neurons (wt 356 ± 11 mV/ms, $n = 22$ vs BACE1 $^{-/-}$ 391 ± 12 mV/ms; $n = 16$, $p = 0.04$, unpaired t test). This finding would be consistent with a recent study reporting enhanced Na^+ currents in acutely isolated hippocampal neurons from BACE1-deficient mice (Hu et al., 2010). Apart from the small acceleration of the upstroke, we did not find appreciable changes in AP amplitude (wt 99.2 ± 0.8 mV vs BACE1 $^{-/-}$ 101.1 ± 0.7 mV, $p = 0.11$), in AP threshold (wt −51.7 ± 0.5 mV vs BACE1 $^{-/-}$ −53.3 ± 0.9 mV, $p = 0.11$), and in AP half-width (wt 1.19 ± 0.02 ms vs BACE1 $^{-/-}$ 1.17 ± 0.02 ms, $p = 0.33$; wt neurons $n = 22$, BACE1 $^{-/-}$ neurons, $n = 16$ for all parameters, unpaired t test). In view of its rather modest effect on AP waveform, enhanced Na^+ current alone cannot account for the altered firing pattern with the prominent loss of adaptation in BACE1-deficient neurons.

Because the features of enhanced excitability in BACE1 $^{-/-}$ neurons during sustained depolarization were well compatible with diminished I_M, we repeated the above experiment in the absence and presence of the KCNQ channel blocker XE991 at a concentration of 10 μM, which is considered selective for KCNQ channels (Wang et al., 1998). XE991 reliably enhanced firing frequency and reduced latency to first spike in wt neurons ($n = 8$), whereas no significant drug response was observed in BACE1 $^{-/-}$ neurons ($n = 5$, Fig. 1*E–H*). Furthermore, XE991 produced a small, but significant, increase in R_N from 275 ± 18 MΩ to 318 ± 23 MΩ in wt neurons ($n = 8$, $p = 0.004$, paired t test). In contrast, R_N was not significantly altered in BACE1 $^{-/-}$ neurons (control, 323 ± 35 MΩ; XE991, 350 ± 33 MΩ, $n = 5$, $p = 0.17$, paired t test).

Because the pharmacological data pointed to a strongly reduced I_M in BACE1-deficient neurons, we directly examined its electrophysiological properties in voltage-clamp recordings from CA1 pyramidal neurons that were acutely isolated from hippocampal slices (Fig. 2*A*, inset). The dissociation procedure has the advantage of truncating most of the extended neurites, thereby yielding much better space-clamp conditions. CA1 pyramidal neurons from the two groups had significantly different zero-current potentials (wt, −65.5 ± 2.9 mV, $n = 11$; BACE1 $^{-/-}$, −53.8 ± 3.1 mV, $n = 12$, $p < 0.05$, unpaired t test). The difference in zero-current potential seems to be in apparent contradiction with our recordings in the slice preparation, where CA1 neurons from wt and BACE1 $^{-/-}$ neurons did not differ in RMP. Because a conditional transgenic suppression of M-channels as well as a spontaneous *Kcnq2* mutation with reduced M-current also failed to alter the resting potential of CA1 neurons when determined in the slice preparation (Peters et al., 2005; Otto et al., 2006), it seems plausible to assume that the acute isolation of the neuron from its surrounding network is likely to accent the contribution of M-current to the control of RMP. In the slice preparation, neurons are subjected to a multitude of synaptic and tonic influences through various transmitters and modulators, which might, directly or indirectly, affect the impact of M-current on RMP. In addition, the dissociation procedure itself, reducing the widely ramified neuron to its somatic region, as well as the recording at room temperature might have produced conditions that foster M-channel activity.

As depicted in Figure 2*A*, 10 μM XE991 produced a depolarizing shift of the zero-current potential that was significantly larger in wt than in BACE1 $^{-/-}$ neurons (wt: ΔV 10.3 ± 1.4 mV, BACE1 $^{-/-}$: ΔV 4.3 ± 0.6 mV, $p < 0.001$, unpaired t test). As a

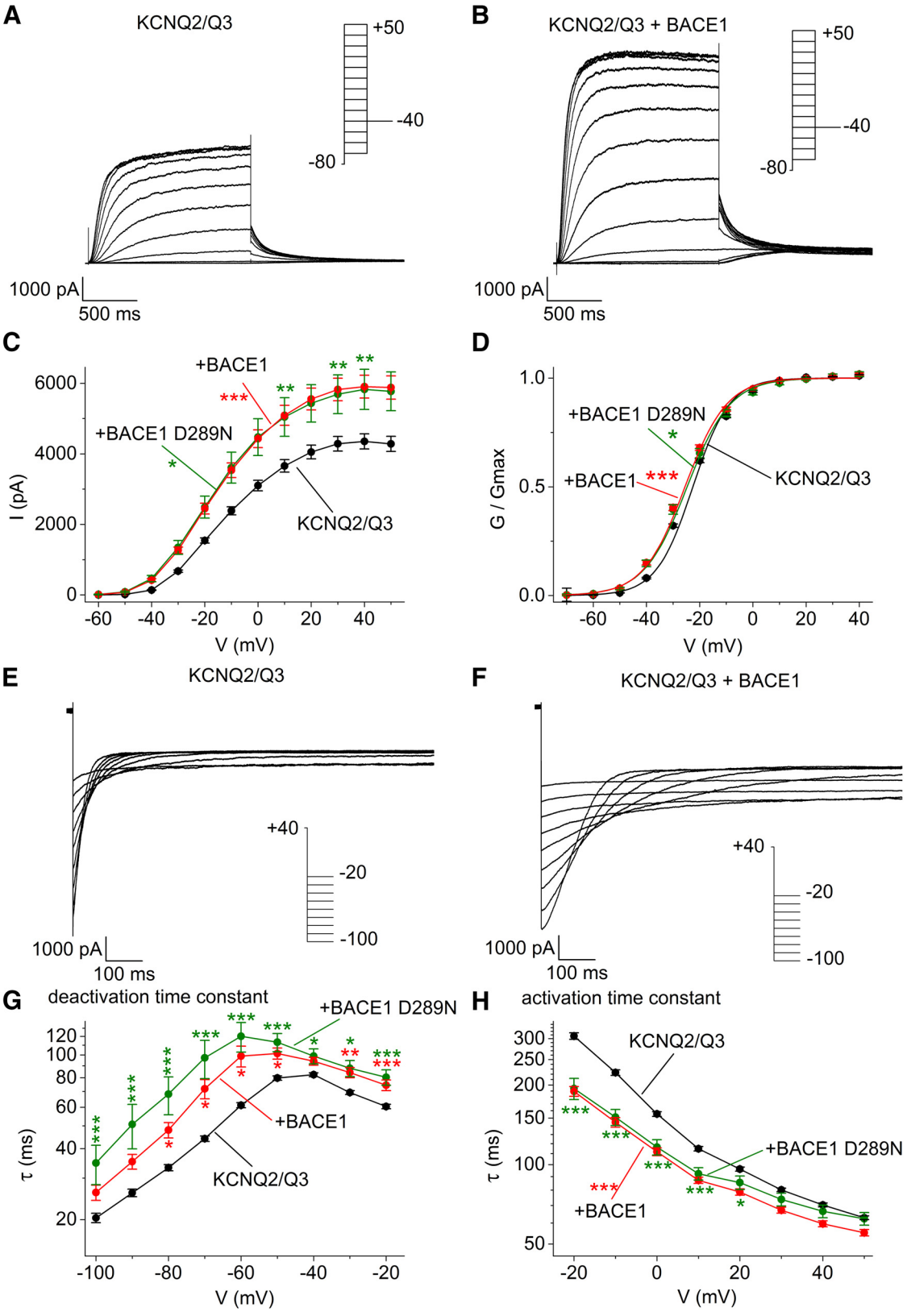

Figure 3. Coexpression of BACE1 increases whole-cell current through heteromeric KCNQ2/Q3 channels in voltage-clamped HEK293T cells. Typical KCNQ2/Q3 current responses to depolarizing voltage steps of increasing amplitude (see insets) were obtained in the absence (***A***) or presence of BACE1 (***B***). ***C***, Using the set of experiments illustrated in ***A***, ***B***, current–voltage (I–V) relationships were determined in which current amplitudes at the end of each step were plotted as function of test potentials in the absence (black data points) and presence of BACE1 (red data points) or its catalytically inactive variant BACE1 D289N (green data points). ***D***, I-V curves of ***C*** were transformed to activation curves, in which normalized conductance was plotted as a function of voltage (see Materials and Methods). Half-activation voltages (V_{mid}) were −22.3 ± 0.3 mV for KCNQ2/Q3 alone (black curve), −26.1 ± 0.5 mV when BACE1 was coexpressed (red curve), and −25.3 ± 0.9 mV when BACE1 D289N was coexpressed (green curve). As indicated by the like-colored asterisks, both BACE1 and BACE1 D289N caused a small, but significant, leftward shift of current activation. Deactivation of KCNQ2/Q3 currents in the absence (***E***) and presence of coexpressed BACE1 (***F***) was determined using a stepwise repolarization protocol (see inset) (*Figure legend continues.*)

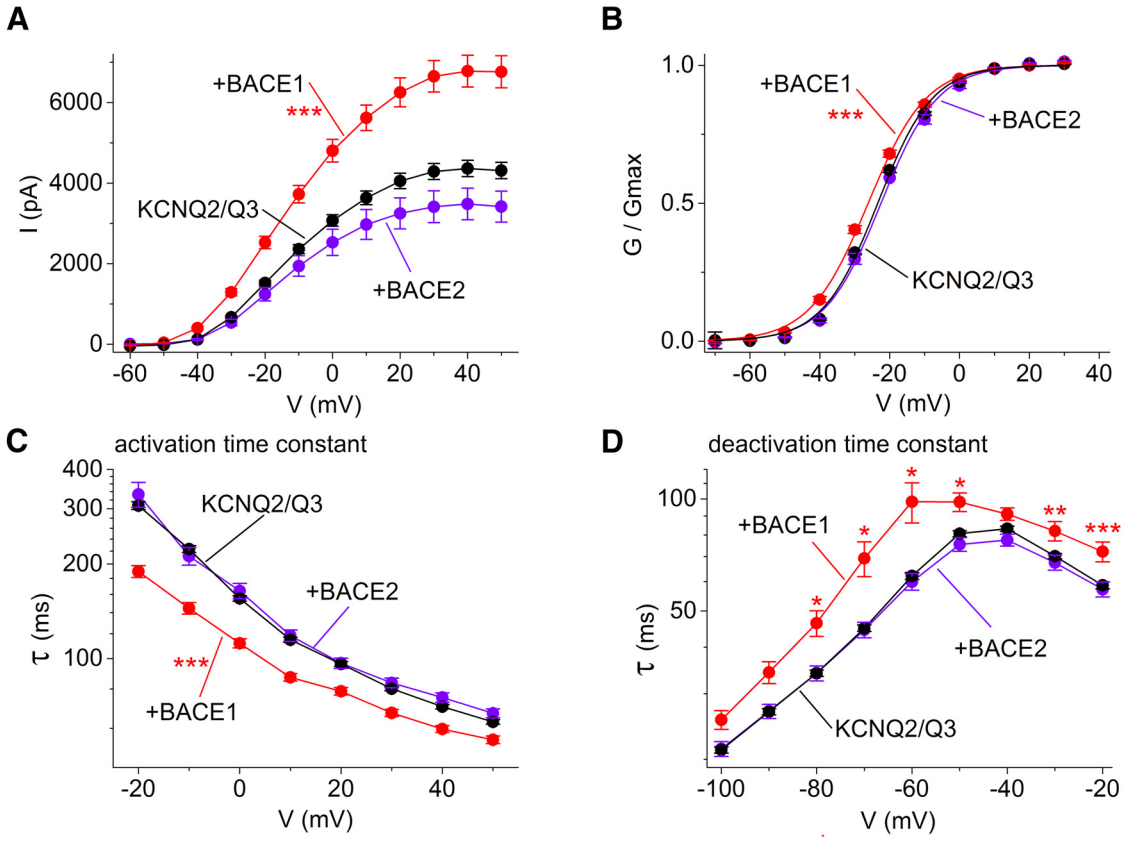

Figure 4. Coexpression of BACE2 in lieu of BACE1 does not alter KCNQ2/Q3 currents of HEK293T cells. All parameters that were affected by BACE1 in previous recordings (red data points) and that are reproduced here from Figure 3 for comparison together with the control data (black data points) remained unchanged in the presence of BACE2 (purple data points), including I-V relationship (***A***), voltage dependence of activation (***B***), time constants of activation (***C***), and deactivation (***D***). KCNQ2/Q3 + BACE2, $n = 27$ (***A–C***), $n = 26$ (***D***). $^{*}p < 0.05$, $^{**}p < 0.01$, $^{***}p < 0.01$, pairwise Mann–Whitney test with Bonferroni correction.

consequence of the pharmacologic suppression of I_M, the zero-current potentials between the two groups were no longer statistically different. We then applied a voltage protocol, in which a standing I_M partially relaxed as the depolarized membrane potential (−30 mV) was repolarized by negative-going voltage steps (−45 to −65 mV). This test protocol was always performed 3 min after whole-cell access had been established and repeated after 10 min of subsequent XE991 application (Fig. 2*B*). Within this voltage range, the hyperpolarization-activated cation current (I_h) is not appreciably activated (Hu et al., 2002). Thus, the slow inward current relaxation upon repolarization should primarily reflect deactivation of I_M. To quantify amplitudes and deactivation time constants of I_M, we subtracted current traces obtained in the absence and presence of XE991. Compared with wt neurons, I_M of BACE1 $^{-/-}$ pyramidal neurons had a much smaller amplitude and decayed much faster (Fig. 2*C*,*D*). It is worth noting that the disruption of *Bace1* altered both amplitude and deactivation kinetics of I_M, whereas a spontaneous *Kcnq2* mutation, which also produced the characteristic impairment in frequency adaptation of hippocampal CA1 neurons, reduced current amplitude without affecting its kinetics (Otto et al., 2006).

←

(*Figure legend continued.*) in high external K^+ solution. ***G***, Current decay was fitted using a mono-exponential function to determine voltage-dependent deactivation kinetics of KCNQ2/Q3 current alone (black data points) and in the presence of coexpressed BACE1 (red data points) or BACE1 D289N (green data points). Like-colored asterisks indicate significant slowing of KCNQ2/Q3 current deactivation when either BACE1 or its inactive variant was present. ***H***, BACE1 and BACE1 D289N accelerated current activation. Activation time constants were obtained by fitting a mono-exponential time course to the rising phase of the current trace in activation experiments of ***A***, ***B***. KCNQ2/Q3, $n = 153$ (***C***, ***D***, ***H***), $n = 138$ (***G***); +BACE1, $n = 116$ (***C***, ***D***, ***H***), $n = 77$ (***G***); +BACE1 D289N, $n = 32$ (***C***, ***D***, ***G***, ***H***). $^{*}p < 0.05$, $^{**}p < 0.01$, $^{***}p < 0.01$, pairwise Mann–Whitney test with Bonferroni correction.

BACE1 amplifies KCNQ2/Q3 currents and alters their kinetics

The electrophysiological recordings from BACE1-deficient neurons strongly suggested that the secretase is required to endow neurons with functionally significant I_M. To explore the mechanism underlying the augmenting effect of BACE1 on neuronal KCNQ channels, we performed whole-cell recordings from HEK293T cells overexpressing KCNQ2/Q3 channels. In a previous study on voltage-dependent Na^+ channels, we had identified both proteolytic and nonproteolytic effects of BACE1 on channel activity (Huth et al., 2009; Huth and Alzheimer, 2012). To determine whether these two fundamentally different modes of action of BACE1 also apply to KCNQ2/Q3 channels, we made use of the BACE1 D289N variant that is rendered enzymatically inactive by an aspartate-to-asparagine mutation in its catalytic center (Huth et al., 2009; Jin et al., 2010).

Consistent with previous reports from heterologous expression systems (Wang et al., 1998), HEK293T cells cotransfected with KCNQ2/Q3 produced a characteristic noninactivating outward current that slowly activated upon depolarization (Fig. 3*A*). Coexpression of BACE1 strongly increased current amplitude and, in the majority of cells, also introduced a mild form of current inactivation at more depolarized command potentials (Fig. 3*B*). The phenomenon of modest current inactivation in the

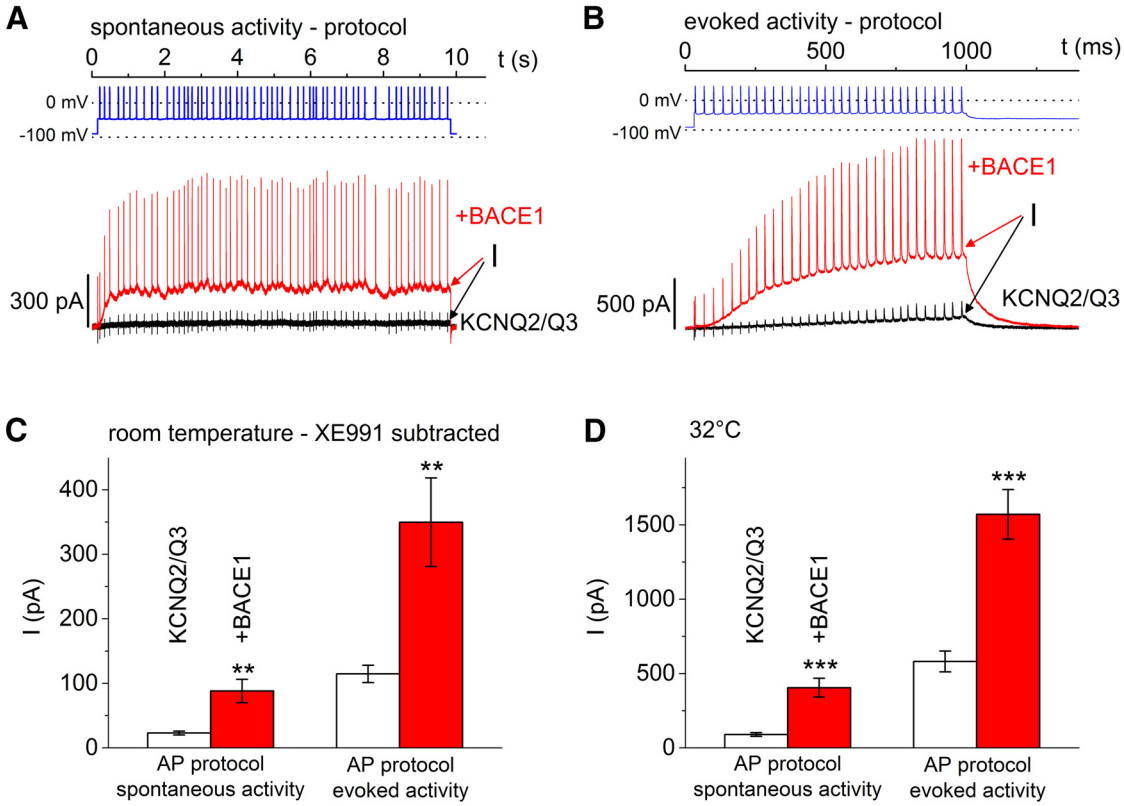

Figure 5. BACE1 amplifies activation of heterologously expressed KCNQ2/Q3 currents during simulated firing patterns. Voltage trajectories obtained from spontaneous (***A***) or evoked firing (***B***) of CA1 pyramidal cells were used as voltage commands in transfected HEK293T cells. Coexpression of BACE1 strongly enhanced KCNQ2/Q3 currents in a frequency-dependent fashion. Note much slower time scale in ***A*** than in ***B***. For quantification, current amplitudes were averaged over the last 50 ms of stimulation (***A***, ***B***, arrows) from recordings performed at room temperature (***C***) or at 32°C (***D***). White columns represent KCNQ2/Q3 alone, $n = 19$ (room temperature), $n = 23$ (32°C); red columns represent KCNQ2/Q3 and BACE1, $n = 17$ (room temperature), $n = 36$ (32°C). $^{**}p < 0.01$, $^{***}p < 0.01$, Mann–Whitney test.

presence of BACE1 was also observed in 13 of 29 recordings performed in high K^+ bath solution (see Materials and Methods), indicating that it was not due to external K^+ accumulation (data not shown). In a small subset of cells (~10%), cotransfection with BACE1 entailed more pronounced inactivation upon strong depolarization (data not shown). The augmenting effect of BACE1 on KCNQ2/Q3 currents did not require proteolysis because its enzymatically inactive mutant produced virtually identical effects on the I/V relationship (Fig. 3*C*). Both BACE1 and its inactive variant produced a small, but significant, leftward shift of the activation curve (Fig. 3*D*).

BACE1 coexpression had also an impact on the gating kinetics of KCNQ2/Q3 channels. In a typical deactivation protocol, where fully activated KCNQ2/Q3 channels were stepwise repolarized to test potentials between −20 and −100 mV, BACE1 caused a pronounced slowing of deactivation kinetics (Fig. 3*E–G*). Again, the effects were reproduced by the BACE1 D289N variant. The same held for the effects of BACE1 on the activation kinetics, which were significantly accelerated by both BACE1 isoforms (Fig. 3*H*).

To demonstrate the specificity of these effects of BACE1 on KCNQ2/Q3 currents, we performed a control experiment in which we examined the currents in HEK293T cells cotransfected with BACE2 in lieu of BACE1. Unlike BACE1, BACE2 did not significantly alter current amplitude and voltage dependence, nor did it affect the activation and deactivation kinetics (Fig. 4).

To explore the functional significance of the data gathered from the expression system, we used voltage trajectories recorded during evoked or spontaneous AP firing of CA1 pyramidal cells as command potentials in voltage-clamped HEK293T cells. XE991 served to isolate KCNQ2/Q3 currents in all experiments made at room temperature. In the absence of BACE1, repetitive AP-like depolarizations activated little KCNQ2/Q3 current (Fig. 5*A–C*, black traces and white columns). With BACE1 cotransfected, however, the same stimulation protocols elicited much more outward current, in particular when the brief depolarizing steps were delivered at high frequency (Fig. 5*B*,*C*, red traces and columns). We replicated these experiments originally made at room temperature, at the temperature used in slice recordings (32°C) and obtained very similar ratios of KCNQ2/Q3 enhancement by BACE1 in the two paradigms (Fig. 5*D*). These findings indicate that, during simulations of physiological firing patterns, the multiple effects of BACE1 on KCNQ2/Q3 channels, including enhanced amplitude, shift of activation, faster kinetics of activation, and slower kinetics of deactivation all lead to a much stronger recruitment of KCNQ2/Q3 current than expected from the increase in current amplitude under steady-state conditions (compare Fig. 3*C*).

Although these data suggest that BACE1 affects primarily the gating properties of KCNQ2/Q3 channels, part of its augmenting effect on steady-state current might still result from enhanced surface expression of channel proteins. To address this question, we performed surface biotinylation assays, which served to quantify KCNQ2/Q3 proteins in terms of surface and total expression (Fig. 6). To underscore the validity of this experiment, we normalized the surface levels of the channel proteins not only to the levels of the commonly used Na^+/K^+-ATPase, but also to cadherin levels, the reason being that the β1-subunit of the Na^+/K^+-

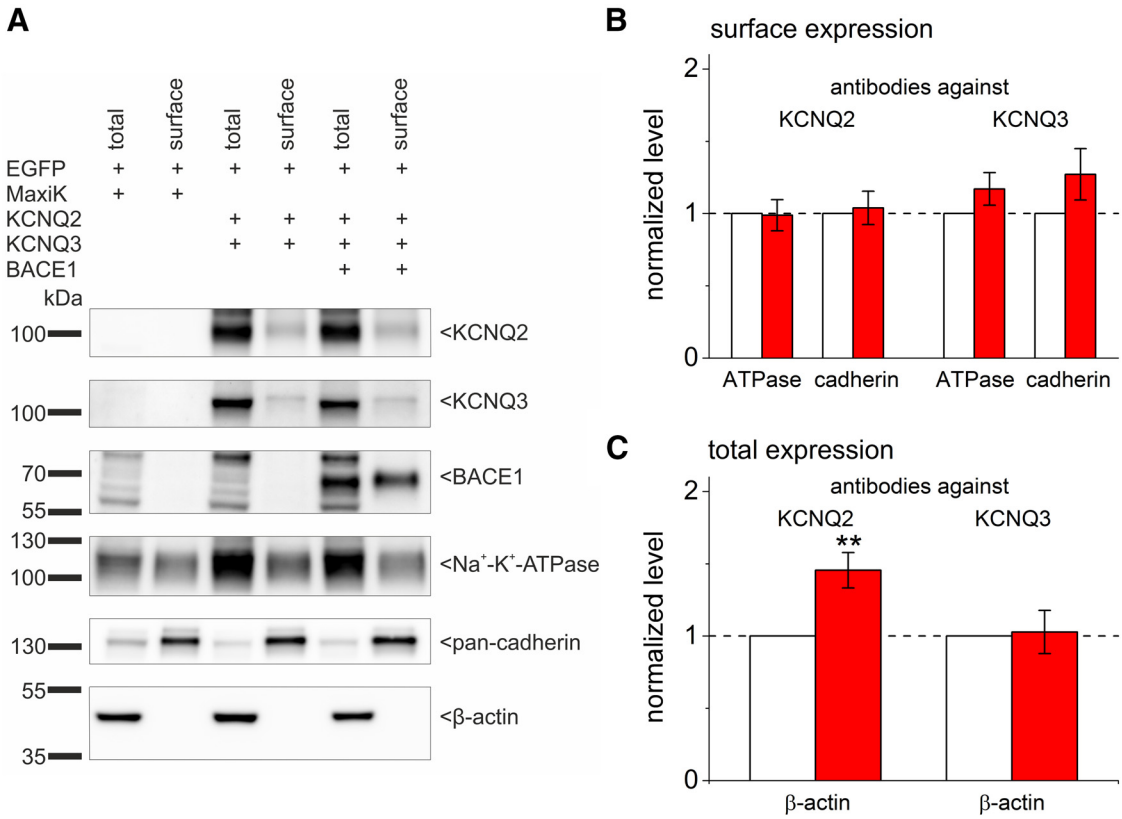

Figure 6. Effects of BACE1 on surface and total levels of KCNQ2 and KCNQ3. ***A***, Western blot of a surface biotinylation of HEK293T cells transfected with KCNQ2 and KCNQ3 with coexpression of BACE1 as indicated above the blot. EGFP and MaxiK served as transfection marker and control, respectively. ***B***, The surface levels of the channel proteins were normalized to the corresponding surface levels of Na^+/K^+-ATPase or cadherin, with the normalized levels determined in the absence of BACE1 set to 1. The histogram shows channel surface levels with BACE1 relative to lanes without BACE1, using antibodies against KCNQ2 and KCNQ3 as indicated above the columns: white column represents transfection with KCNQ2 and KCNQ3; red column represents transfection with KCNQ2, KCNQ3, and BACE1. ***C***, Total protein bands were quantified and normalized to β-actin. $n = 10$. $^{**}p < 0.01$, one-sample *t* test.

ATPase was recently identified as a putative substrate of BACE1 (Kuhn et al., 2012). In this set of experiments, total levels of KCNQ2 but not of KCNQ3 were significantly elevated with BACE1 coexpressed (Fig. 6*C*; $p = 0.005$, one-sample *t* test). In contrast, BACE1 did not alter KCNQ2 levels in the plasma membrane (normalized to Na^+/K^+-ATPase $p = 0.92$, power = 0.05; normalized to cadherin $p = 0.74$, power = 0.06, one-sample *t* test; Fig. 6*B*), nor did it significantly increase KCNQ3 surface expression (normalized to Na^+/K^+-ATPase $p = 0.17$; normalized to cadherin $p = 0.16$, one-sample *t* test; Fig. 6*B*). This finding indicates that surface KCNQ2/Q3 complexes are tightly regulated. Therefore, the increased current with BACE1 can be explained solely with effects on KCNQ2/Q3 gating.

BACE1 interacts with neuronal KCNQ2–5 homotetramers

KCNQ2 and KCNQ3 might also assemble as homotetramers to form functional channels that give rise to I_M. To investigate the interaction between BACE1 and each channel subunit separately, we expressed either of the two KCNQ proteins alone or in combination with BACE1. Consistent with previous work (Wang et al., 1998), homomeric KCNQ2 and KCNQ3 channels exhibited a number of characteristic electrophysiological differences compared with KCNQ2/Q3 heterotetramers: (1) Peak currents of KCNQ2 channels, and much more so of KCNQ3 channels, were substantially reduced (Fig. 7*A–C*). (2) Voltage-dependent activation was shifted to more depolarized potentials for KCNQ2 and to more hyperpolarized potentials for KCNQ3 (Fig. 7*D*). (3) The gating of homomeric channels showed altered activation and deactivation kinetics (data not shown).

Cotransfection with BACE1 did not increase KCNQ3 current amplitudes. BACE1 also produced negligible enhancement (<15% at 0 mV) of the larger currents through the A315T mutant of KCNQ3 (data not shown, see Etxeberria et al., 2004; Zaika et al., 2008). By contrast, KCNQ2 currents were strongly enhanced by BACE1, now attaining amplitudes similar to those of KCNQ2/Q3 heteromers without BACE1 (Fig. 7*C*). BACE1 had no significant effect on the activation curves of either KCNQ2 or KCNQ3 currents (Fig. 7*D*). BACE1 had only minor effects on activation kinetics of KCNQ2 and KCNQ3, but it significantly slowed deactivation kinetics, in particular those of KCNQ3 (data not shown). These data suggest that, although BACE1 interacts with both channel proteins, the majority of its augmenting effect on I_M is most likely mediated by its association with KCNQ2. Because KCNQ5 and KCNQ4 can also contribute to M-current and M-like-current, respectively, we investigated the effects of BACE1 on homomeric channels. In both subtypes, BACE1 produced a strong increase in current amplitude that was comparable with the effects seen in KCNQ2 channels (Fig. 7*E,F*). Assuming that BACE1 enhances neuronal KCNQ2/3 currents not by increasing the number of functional channels in the membrane (see above), but rather by enhancing their open probability, the large increase of homomeric KCNQ2, Q4, and Q5 currents with coexpressed BACE1 goes well along with the low open probabilities of heterologously expressed KCNQ2, Q4, and

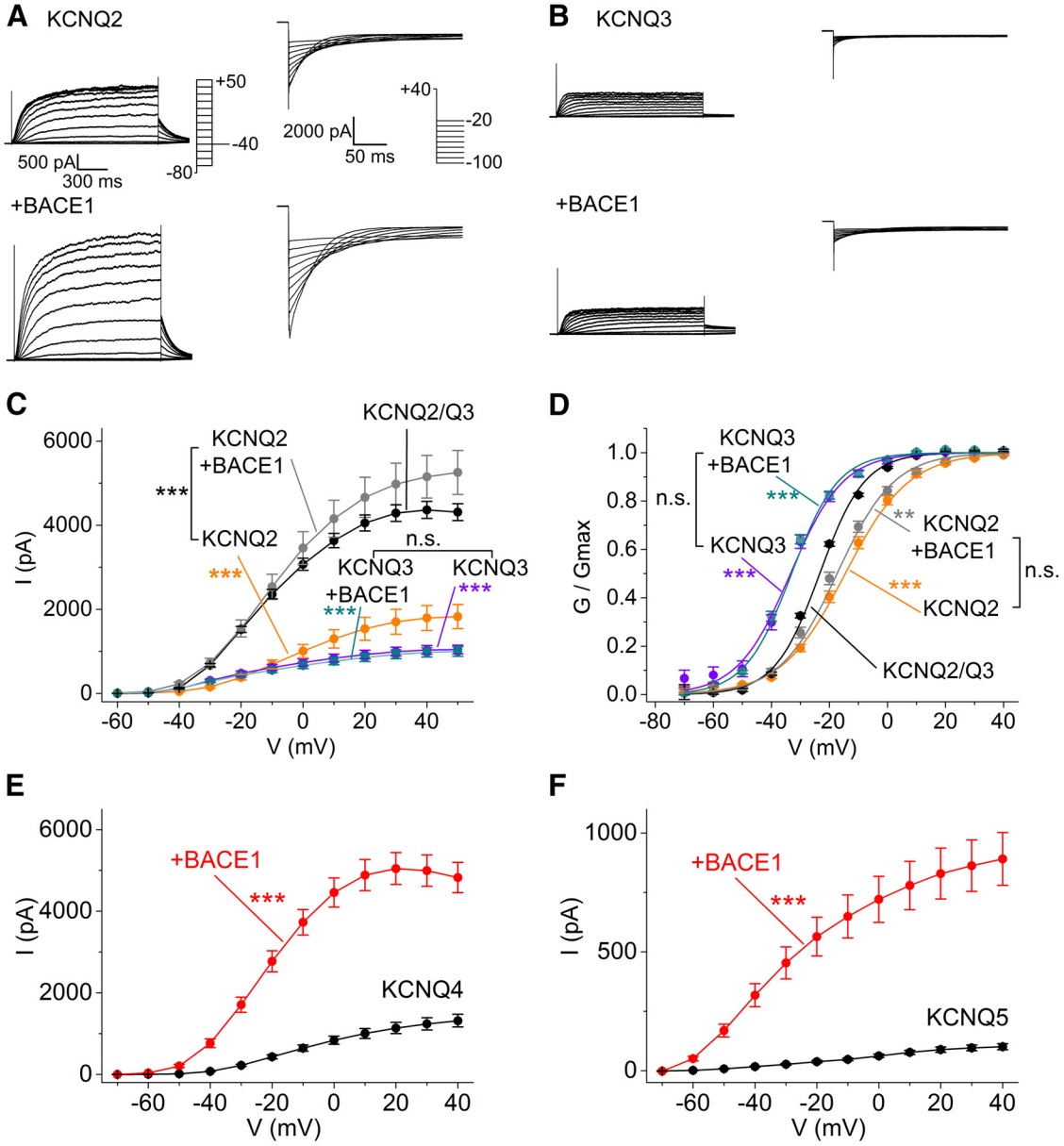

Figure 7. Effects of BACE1 coexpression on activation (***A***, ***B***, left) and deactivation (***A***, ***B***, right) of currents mediated by homomeric KCNQ2 (***A***) or KCNQ3 channels (***B***) in HEK293T cells. From activation protocols, we constructed I-V relationships (***C***) and activation curves (***D***). For comparison, I-V curves and activation curves also include previous results from heteromeric KCNQ2/Q3 (black data points and traces). Half-activation voltages (V_{mid}) were -14.7 ± 1.2 mV for KCNQ2 alone, -17.8 ± 1.2 mV for KCNQ2 and BACE1, -31.1 ± 1.5 mV for KCNQ3 alone, and -32.7 ± 1.2 mV for KCNQ3 and BACE1. KCNQ2, $n = 33$; KCNQ3, $n = 29$; KCNQ2 and BACE1, $n = 38$; KCNQ3 and BACE1, $n = 34$. *$p < 0.05$, **$p < 0.01$, ***$p < 0.01$, pairwise Mann–Whitney test with Bonferroni correction. Coexpression of BACE1 strongly upregulated currents through homomeric KCNQ4 (***E***) and homomeric KCNQ5 (***F***) channels in HEK293T cells. KCNQ4, $n = 34$; KCNQ4 +BACE1, $n = 38$; KCNQ5, $n = 24$; KCNQ5 +BACE1, $n = 29$. ***$p < 0.01$, Mann–Whitney test. n.s., Not significant.

Q5 channels, which were reported to be 0.17, 0.07, and 0.17, respectively (Li et al., 2004, 2005). By contrast, homomeric KCNQ3 channels exhibit a much higher open probability with values between 0.59 (Selyanko et al., 2001) and 0.89 (Li et al., 2004) and, consequently, did not show appreciable increase when BACE1 was coexpressed.

BACE1 does not rescue current decline during PIP_2 depletion

M-channels require a certain level of PtdIns(4,5)P_2 (PIP_2) to open and changes in PIP_2 levels are effective means to regulate I_M (Suh et al., 2006; Hernandez et al., 2008; Telezhkin et al., 2012).

According to the data presented here, BACE1 is another constituent of physiologically sized I_M. To explore the interdependence between these two essential cofactors of proper KCNQ channel gating, we tested whether BACE1 would be capable of counteracting the characteristic current decline when PIP_2 levels fall. We cotransfected HEK293T cells either with the phosphatase construct DR-VSP, which can be activated by strong membrane depolarization, or with its inactive variant DR-VSP-C302S (Hossain et al., 2008; Kruse et al., 2012). The experiment was performed as follows (Fig. 8*A*): Voltage-clamped cells were first subjected to a mild depolarizing voltage step to -20 mV that activated KCNQ2/Q3 current but not the phosphatase, and the current amplitude at the end of this step was determined as I_1. Cells were then depolarized to 100 mV for a variable time period Δt (100–3200 ms) to activate the phosphatase, before the membrane potential was stepped back to -20 mV to obtain a second current reading (I_2). We then calculated the I_2/I_1 ratio as an indi-

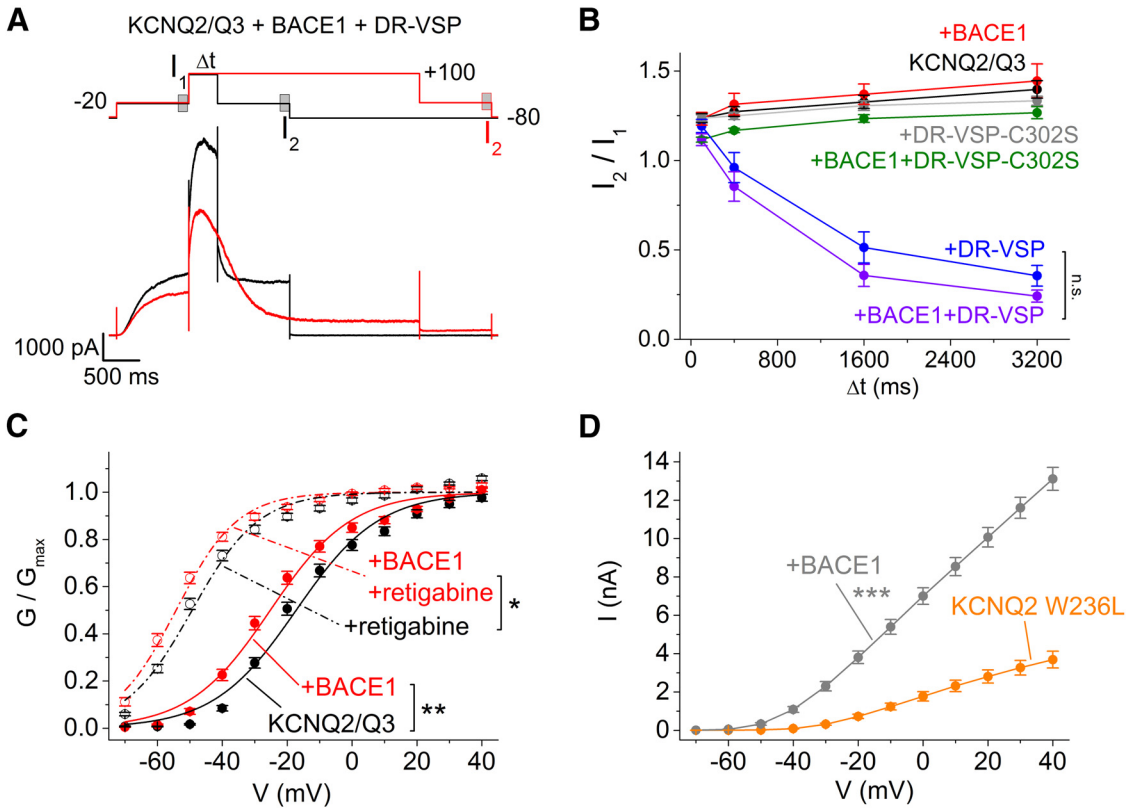

Figure 8. Effects of PIP_2 and retigabine on KCNQ2/Q3 in the absence and presence of BACE1. ***A***, To deplete PIP_2 in a controlled fashion, the voltage-dependent phosphatase DR-VSP was coexpressed with KCNQ2/Q3 alone or together with BACE1 in HEK293T cells. KCNQ2/Q3 currents were measured before (I_1) and after the phosphatase was activated by strong depolarization of variable length (I_2). ***B***, Time course of changes in I_2/I_1 ratio is indicative of current run-down as phosphatase was activated ($n = 15$, blue data points and lines). Coexpression of BACE1 did not attenuate phosphatase-mediated current decline ($n = 19$, purple data points and lines). No changes in I_2/I_1 ratio were observed for currents mediated by KCNQ2/Q3 alone ($n = 15$, black data points and lines), by KCNQ2/Q3 and BACE1 ($n = 20$, red data points and lines), by KCNQ2/Q3 and the inactive phosphatase DR-VSP-C302S ($n = 15$, gray data points and lines), or by KCNQ2/Q3, BACE1, and DR-VSP-C302S ($n = 17$, green data points and lines). ***C***, Responsiveness of KCNQ2/Q3 currents to retigabine (10 μM) is preserved in the presence of BACE1 as indicated by the characteristic drug-induced leftward shift of the activation curves. Maximum current was not enhanced by retigabine (KCNQ2/Q3, $n = 40$; +BACE1, $n = 43$). ***D***, The boosting effect of BACE1 on KCNQ2 current is not impaired when BACE1 is coexpressed with the retigabine-insensitive mutant W236L (KCNQ2 W236L, $n = 26$; +BACE1, $n = 30$). *$p < 0.05$, **$p < 0.01$, ***$p < 0.01$, Mann–Whitney test. n.s., Not significant.

cator of the relative, phosphatase-mediated current decline. In control experiments, the inactive phosphatase construct did not affect the I_2/I_1 ratio, nor did BACE1 or a combination of both (Fig. 8*B*). Once activated, however, the phosphatase caused a decay of the I_2/I_1 ratio. Most importantly, the current decline during PIP_2 depletion proceeded regardless of whether BACE1 was coexpressed or not (Fig. 8*B*). If BACE1 acted predominantly by enhancing the affinity of PIP_2 to the channel, one would have expected a shift in the DR-VSP-induced decay of KCNQ2/Q3 current in the presence of BACE1 because the curves describing the current decay in Figure 8*B* can be understood as a dose–response relationship between PIP_2 level and KCNQ current amplitude. In contrast to some pharmacological enhancers, which were capable of restoring or even potentiating KCNQ current after PIP_2 depletion (Linley et al., 2012; Zhou et al., 2013), BACE1 failed to restore KCNQ2/Q3 current in the absence of adequate PIP_2 binding to the channel.

Retigabine and BACE1 enhance KCNQ2/Q3 current through different mechanisms

Retigabine is an established M-current activator, which enhances the current by shifting the voltage dependence of activation to more negative potentials (Main et al., 2000). To test whether retigabine and BACE1 act at the same or at different sites of the channel protein to enhance the current, we measured activation curves in the absence and presence of coexpressed BACE1 and determined the characteristic shift of the activation curves toward more negative potentials by retigabine (Fig. 8*C*). BACE1 did not abrogate the effect of retigabine, as indicated by the fact that the drug was capable of shifting the activation curve of KCNQ2/Q3 current obtained with BACE1 (Fig. 8*C*). In a second approach, we tested whether BACE1 would enhance KCNQ2 current arising from the retigabine-insensitive mutant W236L (Schenzer et al., 2005; Wuttke et al., 2005). The I/V curves depicted in Figure 8*D* indicate that the efficacy of BACE1 to augment KCNQ2 current was not impaired when the channel was rendered insensitive to retigabine.

BACE1 is physically associated with KCNQ2/Q3 channels

In our electrophysiological experiments, BACE1 upregulated KCNQ2/Q3 currents in a proteolysis-independent fashion that was reminiscent of the well-established boosting effect that the auxiliary KCNE1 subunit exerts on cardiac KCNQ1. To substantiate the hypothesis that the I_M-promoting effect of BACE1 depends on a physical interaction with KCNQ2/Q3 channels, we embarked on two independent strategies: one being coimmunoprecipitation, the other PLA. For coimmunoprecipitation, HEK293T cells were cotransfected with BACE1 constructs with a FLAG-tag and KCNQ constructs with a HA-tag. As depicted in the immunoblot of Figure

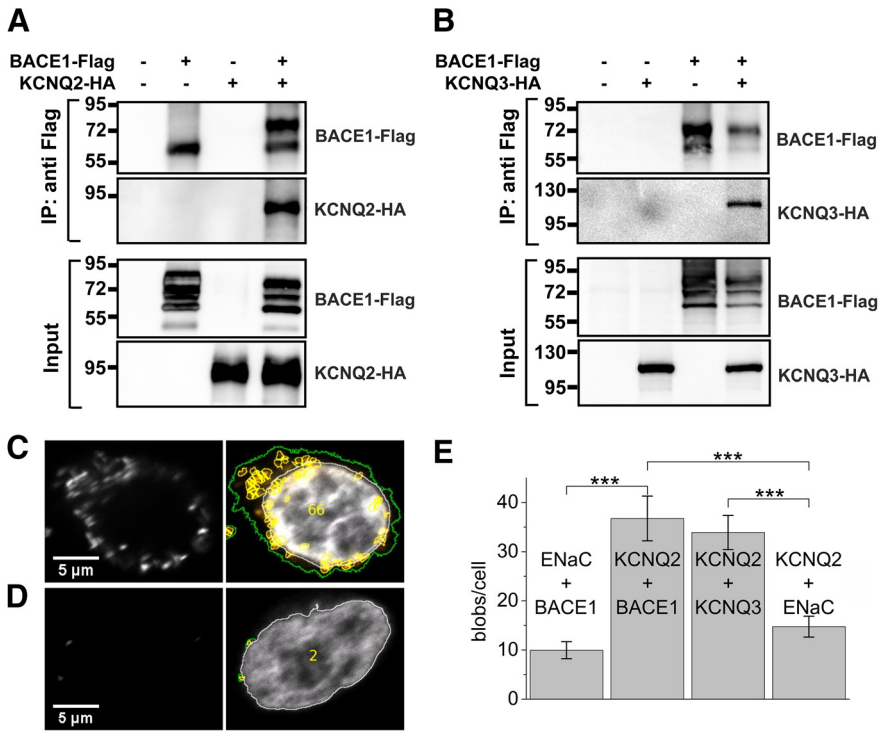

Figure 9. Direct interaction of BACE1 with KCNQ2 and KCNQ3 in HEK293T cells. ***A***, Western blot of a coimmunoprecipitation of KCNQ2 and BACE1 ($n = 3$). ***B***, Western blot of a coimmunoprecipitation of KCNQ3 with BACE1 ($n = 5$). ***C–E***, PLA was performed on HEK293T cells expressing KCNQ2-V5 and BACE1 (***C***) or ENaC-V5 and BACE1 (***D***). Left, Unprocessed data (grayscale, 8 bits). Protein–protein proximity is indicated by bright fluorescent spots. Images were automatically analyzed using the CellProfiler program (right). Nuclei were counterstained with DAPI (gray channel). In a first step, nuclei (white outlines) were identified. The "cell borders" (green outlines) were expanded beyond corresponding PLA signals (orange blobs), if present. In-focus PLA signals were detected (yellow outlines) and counted. Adjacent PLA signals were separated using local intensity maxima. Scale bar, 5 μm. ***E***, Number of PLA signals per cell. $n = 293$ (ENaC-V5 + BACE1), $n = 288$ (KCNQ2-V5 + BACE1), $n = 307$ (KCNQ2-V5 + KCNQ3-HA), $n = 312$ (KCNQ2-V5 + ENaC-HA) from two independent transfections each. $^{***}p < 0.01$, Kruskal–Wallis followed by Mann–Whitney test with Bonferroni correction.

9*A*, *B*, we were able to coprecipitate either KCNQ2 or KCNQ3 with BACE1.

Independent of the immunoblotting experiment, PLA corroborated the close interaction between BACE1 and KCNQ2 channel proteins (Fig. 9*C*). In a control experiment, no such interaction was found between BACE1 and the epithelial sodium channel (ENaC, Fig. 9*D*). In quantitative terms, PLA against KCNQ2-V5 and BACE1 yielded a mean count of 36.7 ± 4.5 blobs per cell ($n = 288$ cells; Fig. 9*E*). As a positive control, PLA against KCNQ2-V5 and coexpressed KCNQ3-HA resulted in 33.9 ± 3.5 blobs per cell ($n = 307$ cells). To control for PLA signals that may arise from unspecific binding of primary antibodies, either BACE1 or KCNQ2-V5 was paired with ENaC as a control partner. ENaC has a similar expression pattern compared with KCNQ2 and was previously shown not to interact with KCNQ2 (Bal et al., 2008). Both samples showed higher counts than the negative control in which KCNQ2-V5 was combined with ENaC-HA (14.7 ± 2.1 blobs per cell, $n = 312$ cells). In a PLA of BACE1 with ENaC-V5, ENaC only fostered 9.9 ± 1.7 blobs per cell ($n = 293$ cells) with BACE1. Two independent lines of biochemical evidence therefore strongly support the notion already suggested from electrophysiology, namely, that the increase of I_M did not result from the shedding of membrane proteins, but from a presumably direct interaction between BACE1 and the channel proteins.

Discussion

We report here that BACE1 is a mandatory constituent of I_M. BACE1-deficient hippocampal neurons exhibited the same features of abnormally enhanced intrinsic excitability that are typically observed in hippocampal neurons with a spontaneous mutation of *Kcnq2* (Otto et al., 2006) or after conditional transgenic suppression of I_M (Peters et al., 2005). Furthermore, voltage-clamp recordings from BACE1$^{-/-}$ neurons directly demonstrated a substantial loss of I_M. Our finding of reduced I_M in BACE1$^{-/-}$ mice should be instrumental to resolve the controversy on the ionic mechanism underlying their susceptibility to seizure-like EEG activity and intermittent convulsions. Whereas Hu et al. (2010) proposed that, in BACE1$^{-/-}$ mice, increased Na^+ channel activity due to enhanced surface levels of Nav1.2 tilts the balance between excitation and inhibition toward an epileptic phenotype, Hitt et al. (2010) found no correlation between Na^+ channel level and seizure activity in BACE1-deficient mice. Mutations in either KCNQ2 or KCNQ3 proteins have been pinpointed as the underlying mechanism of benign familial neonatal convulsions, an autosomal dominant epilepsy of infancy that begins few days after birth and usually disappears within the first year (Jentsch, 2000; Maljevic et al., 2010; Miceli et al., 2011). Because reduced I_M has been well established as an epileptogenic factor in mice and humans, this mechanism should also make a substantial contribution to the seizure proneness of BACE1$^{-/-}$ mice. In view of the multitude of proteins that serve as substrates of BACE1 (Wong et al., 2005; Kuhn et al., 2012), we cannot rule out that future work will reveal additional factors involved in generating this epileptic phenotype, but diminished I_M should stand out as an essential mechanism.

BACE1 as a putative modulatory subunit of KCNQ2/Q3 channel

So far, research in the BACE1 field has focused almost exclusively on the shedding activities of this enzyme and their (patho)physiological sequelae. Studying the interaction of BACE1 with voltage-dependent Na^+ channels, we were the first to demonstrate a physiologically relevant action of BACE1 that occurred independently of protein cleavage (Huth et al., 2009). Here, we extend this novel principle of BACE1 function to the KCNQ family. Importantly, BACE1 not only augments steady-state I_M but also accelerates its activation and slows its deactivation. The effects of BACE1 on gating kinetics are particularly important to strengthen the impact of I_M on neuronal activity during resonance behavior and frequency adaptation.

Whereas the electrophysiological recordings in the heterologous expression system demonstrated that the effects of BACE1 on KCNQ2/Q3 currents can be recapitulated by its proteolytically inactive variant BACE1 D289N, thereby pointing to a nonenzymatic action, it was two independent protein interaction experiments (i.e., coimmunoprecipitation and PLA) that strongly

argued in favor of a direct physical interaction between BACE1 and the channel proteins. Unlike cardiac KCNQ1 channels, which assemble with KCNE1 subunits to supply functional I_{KS} to heart cells, neuronal KCNQ channels have been thought to operate without auxiliary β-subunits (Brown and Passmore, 2009). Given that BACE1, like KCNE1, is a Type I transmembrane protein and that both show equally augmenting effects on channel activity, it is well conceivable that the role of BACE1 for neuronal KCNQ2/Q3 channels is akin to that of KCNE1 for cardiac KCNQ1 channels.

Implications for Alzheimer's disease

What does the surprising interaction between BACE1 and neuronal KCNQ channels tell us about their roles in AD and their suitability as therapeutic targets? Early animal studies raised hope that I_M inhibitors might improve learning and memory deficits, but in subsequent clinical trials, the M-channel blocker linopirdine failed to ameliorate memory deficits in older adults and this treatment option has been abandoned since (Wulff et al., 2009). A recent study on aged primates showed that injection of the M-channel blocker XE991 in the prefrontal cortex restored the neuronal substrate of retention in a working memory test (Wang et al., 2011). The authors proposed that this age-related change in cortical information processing might render the brain particularly vulnerable to AD. Does this finding reinstate KCNQ channels as a promising target for second generation M-channel inhibitors? There is a strong caveat to this implication because inhibition of I_M might induce or exacerbate seizure activity in AD patients. Compared with an age-matched control group in good mental health, AD patients exhibit a much higher propensity to develop seizure activity that often remains clinically undetected (Vossel et al., 2013). Importantly, aberrant network activity is not an accompanying symptom, but an essential feature of AD, as it is capable of propelling neurodegeneration (Huang and Mucke, 2012). Lending support to the hypothesis that hyperexcitability is causally linked to the cognitive decline in AD, Sanchez et al. (2012) reported recently that suppression by leviracetam of abnormal spikes in EEG recordings reversed synaptic dysfunction and learning and memory deficits in an animal model of AD. In light of this novel concept of how AD develops and proceeds, our finding that BACE1 augments I_M suggests that the upregulation of BACE1 in brains of patients with mild cognitive impairments and AD (Cheng et al., 2014) might also serve to strengthen an endogenous anticonvulsant mechanism. Although this putative compensatory mechanism is obviously doomed to fail, it might perhaps slow the progression from mild cognitive impairment to overt dementia. This would further argue against inhibition of I_M as a therapeutic option in AD.

On a cautionary note, the decrease of I_M in BACE1-deficient neurons does not necessarily imply the reverse, namely, a boost of I_M when BACE1 activity exceeds physiological levels, as it does in AD. As long as type, subcellular site, and mechanism of interaction between neuronal KCNQ channel complexes and BACE1 as well as their exact stoichiometry remain unknown, we cannot exclude that physiological BACE1 levels already increase I_M in a saturating fashion. In any case, the fact that BACE1 augments I_M in a proteolysis-independent manner should offer good news for treatment strategies aiming at reducing enzymatic activity by pharmacological means. Such BACE1 inhibitors might suppress its amyloidogenic effects while at the same time preserving its beneficial nonenzymatic actions on I_M.

References

Bal M, Zhang J, Zaika O, Hernandez CC, Shapiro MS (2008) Homomeric and heteromeric assembly of KCNQ (Kv7) K^+ channels assayed by total internal reflection fluorescence/fluorescence resonance energy transfer and patch clamp analysis. J Biol Chem 283:30668–30676. CrossRef Medline

Battefeld A, Tran BT, Gavrilis J, Cooper EC, Kole MH (2014) Heteromeric Kv7.2/7.3 channels differentially regulate action potential initiation and conduction in neocortical myelinated axons. J Neurosci 34:3719–3732. CrossRef Medline

Brown DA, Adams PR (1980) Muscarinic suppression of a novel voltage-sensitive K^+ current in a vertebrate neurone. Nature 283:673–676. CrossRef Medline

Brown DA, Passmore GM (2009) Neural KCNQ (Kv7) channels. Br J Pharmacol 156:1185–1195. CrossRef Medline

Carpenter AE, Jones TR, Lamprecht MR, Clarke C, Kang IH, Friman O, Guertin DA, Chang JH, Lindquist RA, Moffat J, Golland P, Sabatini DM (2006) CellProfiler: image analysis software for identifying and quantifying cell phenotypes. Genome Biol 7:R100. CrossRef Medline

Cheng X, He P, Lee T, Yao H, Li R, Shen Y (2014) High activities of BACE1 in brains with mild cognitive impairment. Am J Pathol 184:141–147. CrossRef Medline

Dominguez D, Tournoy J, Hartmann D, Huth T, Cryns K, Deforce S, Serneels L, Camacho IE, Marjaux E, Craessaerts K, Roebroek AJ, Schwake M, D'Hooge R, Bach P, Kalinke U, Moechars D, Alzheimer C, Reiss K, Saftig P, De Strooper B (2005) Phenotypic and biochemical analyses of BACE1- and BACE2-deficient mice. J Biol Chem 280:30797–30806. CrossRef Medline

Etxeberria A, Santana-Castro I, Regalado MP, Aivar P, Villarroel A (2004) Three mechanisms underlie KCNQ2/3 heteromeric potassium M-channel potentiation. J Neurosci 24:9146–9152. CrossRef Medline

Guan D, Higgs MH, Horton LR, Spain WJ, Foehring RC (2011) Contributions of Kv7-mediated potassium current to sub- and suprathreshold responses of rat layer II/III neocortical pyramidal neurons. J Neurophysiol 106:1722–1733. CrossRef Medline

Gu N, Vervaeke K, Hu H, Storm JF (2005) Kv7/KCNQ/M and HCN/h, but not KCa2/SK channels, contribute to the somatic medium after-hyperpolarization and excitability control in CA1 hippocampal pyramidal cells. J Physiol 566:689–715. CrossRef Medline

Hernandez CC, Zaika O, Shapiro MS (2008) A carboxy-terminal inter-helix linker as the site of phosphatidylinositol 4,5-bisphosphate action on Kv7 (M-type) K^+ channels. J Gen Physiol 132:361–381. CrossRef Medline

Hitt BD, Jaramillo TC, Chetkovich DM, Vassar R (2010) BACE1 $^{-/-}$ mice exhibit seizure activity that does not correlate with sodium channel level or axonal localization. Mol Neurodegener 5:31. CrossRef Medline

Hossain MI, Iwasaki H, Okochi Y, Chahine M, Higashijima S, Nagayama K, Okamura Y (2008) Enzyme domain affects the movement of the voltage sensor in ascidian and zebrafish voltage-sensing phosphatases. J Biol Chem 283:18248–18259. CrossRef Medline

Hu H, Vervaeke K, Storm JF (2002) Two forms of electrical resonance at theta frequencies, generated by M-current, h-current and persistent Na^+ current in rat hippocampal pyramidal cells. J Physiol 545:783–805. CrossRef Medline

Hu H, Vervaeke K, Storm JF (2007) M-channels (Kv7/KCNQ channels) that regulate synaptic integration, excitability, and spike pattern of CA1 pyramidal cells are located in the perisomatic region. J Neurosci 27:1853–1867. CrossRef Medline

Hu X, Zhou X, He W, Yang J, Xiong W, Wong P, Wilson CG, Yan R (2010) BACE1 deficiency causes altered neuronal activity and neurodegeneration. J Neurosci 30:8819–8829. CrossRef Medline

Huang Y, Mucke L (2012) Alzheimer mechanisms and therapeutic strategies. Cell 148:1204–1222. CrossRef Medline

Huth T, Alzheimer C (2012) Voltage-dependent Na^+ channels as targets of BACE1-Implications for neuronal firing and beyond. Curr Alzheimer Res 9:184–188. CrossRef Medline

Huth T, Schmidt-Neuenfeldt K, Rittger A, Saftig P, Reiss K, Alzheimer C (2009) Non-proteolytic effect of beta-site APP-cleaving enzyme 1 (BACE1) on sodium channel function. Neurobiol Dis 33:282–289. CrossRef Medline

Jentsch TJ (2000) Neuronal KCNQ potassium channels: physiology and role in disease. Nat Rev Neurosci 1:21–30. CrossRef Medline

Jin S, Agerman K, Kolmodin K, Gustafsson E, Dahlqvist C, Jureus A, Liu G, Fälting J, Berg S, Lundkvist J, Lendahl U (2010) Evidence for dimeric BACE-mediated APP processing. Biochem Biophys Res Commun 393:21–27. CrossRef Medline

Kruse M, Hammond GR, Hille B (2012) Regulation of voltage-gated potassium channels by PI(4,5)P2. J Gen Physiol 140:189–205. CrossRef Medline

Kuhn PH, Koroniak K, Hogl S, Colombo A, Zeitschel U, Willem M, Volbracht C, Schepers U, Imhof A, Hoffmeister A, Haass C, Roßner S, Bräse S, Lichtenthaler SF (2012) Secretome protein enrichment identifies physiological BACE1 protease substrates in neurons. EMBO J 31:3157–3168. CrossRef Medline

Leitner MG, Feuer A, Ebers O, Schreiber DN, Halaszovich CR, Oliver D (2012) Restoration of ion channel function in deafness-causing KCNQ4 mutants by synthetic channel openers. Br J Pharmacol 165:2244–2259. CrossRef Medline

Lerche C, Scherer CR, Seebohm G, Derst C, Wei AD, Busch AE, Steinmeyer K (2000) Molecular cloning and functional expression of KCNQ5, a potassium channel subunit that may contribute to neuronal M-current diversity. J Biol Chem 275:22395–22400. CrossRef Medline

Li Y, Gamper N, Shapiro MS (2004) Single-channel analysis of KCNQ K^+ channels reveals the mechanism of augmentation by a cysteine-modifying reagent. J Neurosci 24:5079–5090. CrossRef Medline

Li Y, Gamper N, Hilgemann DW, Shapiro MS (2005) Regulation of Kv7 (KCNQ) K^+ channel open probability by phosphatidylinositol 4,5-bisphosphate. J Neurosci 25:9825–9835. CrossRef Medline

Linley JE, Pettinger L, Huang D, Gamper N (2012) M channel enhancers and physiological M channel block. J Physiol 590:793–807. CrossRef Medline

Main MJ, Cryan JE, Dupere JR, Cox B, Clare JJ, Burbidge SA (2000) Modulation of KCNQ2/3 potassium channels by the novel anticonvulsant retigabine. Mol Pharmacol 58:253–262. CrossRef Medline

Maljevic S, Wuttke TV, Seebohm G, Lerche H (2010) KV7 channelopathies. Pflugers Arch 460:277–288. CrossRef Medline

Martire M, Castaldo P, D'Amico M, Preziosi P, Annunziato L, Taglialatela M (2004) M channels containing KCNQ2 subunits modulate norepinephrine, aspartate, and GABA release from hippocampal nerve terminals. J Neurosci 24:592–597. CrossRef Medline

Miceli F, Soldovieri MV, Iannotti FA, Barrese V, Ambrosino P, Martire M, Cilio MR, Taglialatela M (2011) The voltage-sensing domain of K(v)7.2 channels as a molecular target for epilepsy-causing mutations and anticonvulsants. Front Pharmacol 2:2. CrossRef Medline

Otto JF, Yang Y, Frankel WN, White HS, Wilcox KS (2006) A spontaneous mutation involving Kcnq2 (Kv7.2) reduces M-current density and spike frequency adaptation in mouse CA1 neurons. J Neurosci 26:2053–2059. CrossRef Medline

Passmore GM, Reilly JM, Thakur M, Keasberry VN, Marsh SJ, Dickenson AH, Brown DA (2012) Functional significance of M-type potassium channels in nociceptive cutaneous sensory endings. Front Mol Neurosci 5:63. CrossRef Medline

Peters HC, Hu H, Pongs O, Storm JF, Isbrandt D (2005) Conditional transgenic suppression of M channels in mouse brain reveals functions in neuronal excitability, resonance and behavior. Nat Neurosci 8:51–60. CrossRef Medline

Sanchez PE, Zhu L, Verret L, Vossel KA, Orr AG, Cirrito JR, Devidze N, Ho K, Yu GQ, Palop JJ, Mucke L (2012) Levetiracetam suppresses neuronal network dysfunction and reverses synaptic and cognitive deficits in an Alzheimer's disease model. Proc Natl Acad Sci U S A 109:E2895–E2903. CrossRef Medline

Sanguinetti MC, Curran ME, Zou A, Shen J, Spector PS, Atkinson DL, Keating MT (1996) Coassembly of K(V)LQT1 and minK (IsK) proteins to form cardiac I(Ks) potassium channel. Nature 384:80–83. CrossRef Medline

Schenzer A, Friedrich T, Pusch M, Saftig P, Jentsch TJ, Grötzinger J, Schwake M (2005) Molecular determinants of KCNQ (Kv7) K^+ channel sensitivity to the anticonvulsant retigabine. J Neurosci 25:5051–5060. CrossRef Medline

Schroeder BC, Hechenberger M, Weinreich F, Kubisch C, Jentsch TJ (2000) KCNQ5, a novel potassium channel broadly expressed in brain, mediates M-type currents. J Biol Chem 275:24089–24095. CrossRef Medline

Schwake M, Athanasiadu D, Beimgraben C, Blanz J, Beck C, Jentsch TJ, Saftig P, Friedrich T (2006) Structural determinants of M-type KCNQ (Kv7) K^+ channel assembly. J Neurosci 26:3757–3766. CrossRef Medline

Selyanko AA, Hadley JK, Brown DA (2001) Properties of single M-type KCNQ2/KCNQ3 potassium channels expressed in mammalian cells. J Physiol 534:15–24. CrossRef Medline

Shah MM, Migliore M, Brown DA (2011) Differential effects of Kv7 (M-) channels on synaptic integration in distinct subcellular compartments of rat hippocampal pyramidal neurons. J Physiol 589:6029–6038. CrossRef Medline

Shah M, Mistry M, Marsh SJ, Brown DA, Delmas P (2002) Molecular correlates of the M-current in cultured rat hippocampal neurons. J Physiol 544:29–37. CrossRef Medline

Söderberg O, Gullberg M, Jarvius M, Ridderstråle K, Leuchowius KJ, Jarvius J, Wester K, Hydbring P, Bahram F, Larsson LG, Landegren U (2006) Direct observation of individual endogenous protein complexes in situ by proximity ligation. Nat Methods 3:995–1000. CrossRef Medline

Suh BC, Inoue T, Meyer T, Hille B (2006) Rapid chemically induced changes of PtdIns(4,5)P2 gate KCNQ ion channels. Science 314:1454–1457. CrossRef Medline

Sun J, Kapur J (2012) M-type potassium channels modulate Schaffer collateral-CA1 glutamatergic synaptic transmission. J Physiol 590:3953–3964. CrossRef Medline

Telezhkin V, Reilly JM, Thomas AM, Tinker A, Brown DA (2012) Structural requirements of membrane phospholipids for M-type potassium channel activation and binding. J Biol Chem 287:10001–10012. CrossRef Medline

Tzingounis AV, Nicoll RA (2008) Contribution of KCNQ2 and KCNQ3 to the medium and slow afterhyperpolarization currents. Proc Natl Acad Sci U S A 105:19974–19979. CrossRef Medline

Vassar R, Kuhn PH, Haass C, Kennedy ME, Rajendran L, Wong PC, Lichtenthaler SF (2014) Function, therapeutic potential and cell biology of BACE proteases: current status and future prospects. J Neurochem 130:4–28. CrossRef Medline

Vervaeke K, Gu N, Agdestein C, Hu H, Storm JF (2006) Kv7/KCNQ/M-channels in rat glutamatergic hippocampal axons and their role in regulation of excitability and transmitter release. J Physiol 576:235–256. CrossRef Medline

Vossel KA, Beagle AJ, Rabinovici GD, Shu H, Lee SE, Naasan G, Hegde M, Cornes SB, Henry ML, Nelson AB, Seeley WW, Geschwind MD, Gorno-Tempini ML, Shih T, Kirsch HE, Garcia PA, Miller BL, Mucke L (2013) Seizures and epileptiform activity in the early stages of Alzheimer disease. JAMA Neurol 70:1158–1166. CrossRef Medline

Wang HS, Pan Z, Shi W, Brown BS, Wymore RS, Cohen IS, Dixon JE, McKinnon D (1998) KCNQ2 and KCNQ3 potassium channel subunits: molecular correlates of the M-channel. Science 282:1890–1893. CrossRef Medline

Wang M, Gamo NJ, Yang Y, Jin LE, Wang XJ, Laubach M, Mazer JA, Lee D, Arnsten AF (2011) Neuronal basis of age-related working memory decline. Nature 476:210–213. CrossRef Medline

Wong HK, Sakurai T, Oyama F, Kaneko K, Wada K, Miyazaki H, Kurosawa M, De Strooper B, Saftig P, Nukina N (2005) Beta subunits of voltage-gated sodium channels are novel substrates of beta-site amyloid precursor protein-cleaving enzyme (BACE1) and gamma-secretase. J Biol Chem 280:23009–23017. CrossRef Medline

Wulff H, Castle NA, Pardo LA (2009) Voltage-gated potassium channels as therapeutic targets. Nat Rev Drug Discov 8:982–1001. CrossRef Medline

Wuttke TV, Seebohm G, Bail S, Maljevic S, Lerche H (2005) The new anticonvulsant retigabine favors voltage-dependent opening of the Kv7.2 (KCNQ2) channel by binding to its activation gate. Mol Pharmacol 67:1009–1017. CrossRef Medline

Yan R, Vassar R (2014) Targeting the beta secretase BACE1 for Alzheimer's disease therapy. Lancet Neurol 13:319–329. CrossRef Medline

Yue C, Yaari Y (2006) Axo-somatic and apical dendritic Kv7/M channels differentially regulate the intrinsic excitability of adult rat CA1 pyramidal cells. J Neurophysiol 95:3480–3495. CrossRef Medline

Zaika O, Hernandez CC, Bal M, Tolstykh GP, Shapiro MS (2008) Determinants within the turret and pore-loop domains of KCNQ3 K^+ channels governing functional activity. Biophys J 95:5121–5137. CrossRef Medline

Zhou P, Yu H, Gu M, Nan FJ, Gao Z, Li M (2013) Phosphatidylinositol 4,5-bisphosphate alters pharmacological selectivity for epilepsy-causing KCNQ potassium channels. Proc Natl Acad Sci U S A 110:8726–8731. CrossRef Medline